Passive Alignment Principle for Robotic Assembly Between a Ring and a Shaft With Extremely Narrow Clearance

Junji Takahashi, *Member, IEEE*, Tomoya Fukukawa, and Toshio Fukuda, *Fellow, IEEE*

***Abstract*—This paper deals with precise insertion processing (peg-in-hole task) for speeding up and increasing flexibility of assembly process in factory automation. When a gap between a peg and a hole is narrower than positioning accuracy of robotic manipulator, it is impossible to succeed the peg-in-hole task by conventional position control methods. Moreover, in the case that a robotic hand holds a deformable thin ring and put it around a shaft, the insertion process becomes increasingly difficult because the gripping force deforms the ring and the narrow gap is crushed. We propose a novel mating technique based on passive alignment principle (PAP) in order to solve the twin problems of accuracy and deformation. The PAP mechanism can correct the ring position in nanoorder and remove the ring deformation. We derived the limitations of the PAP, which are remaining position errors after the PAP applied, based on Hertz stress. We also analyzed accuracy requirements of industrial robotic manipulator for applying the PAP and calculated allowance diagrams. We conducted 280 mating and insertion experiments with four kinds of materials of rings and shafts with three different insertion directions. The success rate 97.8% validates our proposed PAP-based mating algorithm.**

***Index Terms*—Close tolerances fit, Hertz contact stress, peg-in-hole, robotic assembly.**

I. Introduction

ROBOTIC assembly is one of the most important processes in factory automation. The robotic assembly is repeated many times in many situations and has a great influence on the cost, on the manufacturing time, and also on the quality of products. The current trends of end products are close packed as well as downsizing that would require the precise assembly methods. In the recent report, the desired assembly accuracy is extremely high [1], for instance, the clearance between the peg and hole is 9 μm (50 H8/50 g7). The downsizing of products induces thinning of parts and causes a deformation problem during assembly. In the case that a robotic hand holds a deformable thin ring and put it around a shaft, the insertion process becomes increasingly difficult because the gripping force deforms the ring and the narrowest clearance is crushed.

On the other hand, future production systems are expected to cope with manufacturing of wide variety of products in small quantities [2], [3]. The most effective solution for this requirement is an intelligent manufacturing which can automatically adapt to changing environments and varying process requirements. In order to keep the flexibility in manufacturing, the intelligent manufacturing-based production systems should include as few special processes as possible, which are realized by specialized robotic systems or skillful human workers. In other words, automated production systems should be reorganized with versatile robot systems, such as a 6-DOF robot manipulator and a multifingered robotic hand.

According to our own survey, the positioning repeatability of the most accurate 6-DOF robotic manipulator in the world is ± 0.010 mm (see Table I). Therefore, the peg-in-hole task with clearance which is smaller than 20 μm cannot be succeeded by any manipulators with conventional position control. In order to succeed the peg-in-hole task with extremely narrow clearance by the 6-DOF robotic manipulator, a new automatic precise mating and insertion method would be necessary.

Whitney gave kinematic analyses of the peg-in-hole problem and proved that the jamming and wedging could be avoided by placing the compliance center at or near the tip of the peg [4]. A remote center compliance (RCC) device, which realizes the compliance effect passively, has been put for practical use and been studied for long time [5]–[8]. The RCC device, however,

TABLE I
The Positional Repeatability of Major Industrial Robots Around the World

Manufacture	Nationality	Series	Pose Repeatability
KUKA	Germany	KR6R900	± 0.030 mm
ABB	Switzerland	IRB120	± 0.010 mm
STAUBLI	Switzerland	TX40	± 0.020 mm
FANUC	Japan	LR MATE	± 0.020 mm
MITSUBISHI	Japan	RV2	± 0.020 mm
TOSHIBA	Japan	TV800	± 0.020 mm
DENSO	Japan	VP-G	± 0.020 mm
YASKAWA	Japan	MOTOMAN-MHJ	± 0.030 mm

Manuscript received March 31, 2014; revised February 28, 2015; accepted May 23, 2015. Date of publication June 23, 2015; date of current version February 12, 2016. Recommended by Technical Editor H. Ding.

J. Takahashi is with the Department of Integrated Information Technology, College of Science and Engineering, Aoyama Gakuin University, Sagamihara 252-5258, Japan (e-mail: takahashi@it.aoyama.ac.jp).

T. Fukukawa is with the Department of Mechanical Science and Engineering, Graduate School of Engineering, Nagoya University, Nagoya 464-8603, Japan (e-mail: fukukawa@robo.mein.nagoya-u.ac.jp).

T. Fukuda is with the Department of Mechatronics Engineering, Graduate School of Science and Technology, Meijo University, Nagoya 468-8502, Japan (e-mail: tofukuda@meijo-u.ac.jp).

This paper has supplementary downloadable material available at http://ieeexplore.ieee.orgprovided by the authors. This includes a video in MP4, which shows PAP insertion. This material is 13.2 MB. Contact takahashi@it.aoyama.ac.jp for further questions about this work.

Color versions of one or more of the figures in this paper are available online at http://ieeexplore.ieee.org.

Digital Object Identifier 10.1109/TMECH.2015.2448639

has the following problems: it cannot be applied for a hole part that has no or too small chamfer because the RCC effects the peg part when they contact each other on their own chamfer, and it cannot be applied for a nonvertical insertion direction because the RCC device holds the peg part with hanging by elastic elements.

Active compliance, using force feedback control, has also been studied extensively. The first interaction control of manipulator was given as *hybrid position/force control* [9]. How to apply the hybrid control to a peg-in-hole problem was introduced in detail in [10]. Then the *impedance control* [11], which enables a robot manipulator to maneuver in a constrained environment maintaining adequate contact forces, was proposed. Koide applied *impedance control* to the peg-in-hole task and succeeded on the condition that the clearance was $40\,\mu$m [12]. Joo proposed a mating algorithm that sequentially explores fine geometrical relations of peg and hole based on the direction of contact force and succeeded when the clearance was $10\,\mu$m [13] by the 4-DOF manipulator. Tsumugiwa proposed a control strategy for the human–robot cooperation in the peg-in-hole task. This strategy ensured the success of the case that the clearance was $30\,\mu$m [14]. Before now, the peg-in-hole task with the clearance smaller than $10\,\mu$m has not been succeeded by the 6-DOF manipulator. Furthermore , these strategies including force feedback control are not suitable for speeding up because they need a parameter tuning phase of "try and error" before running. Although the issue of automatic parameter optimization has studied from several aspects [15]–[17], they still need more than several tens of seconds for parameter tuning and do not reach fundamental solution.

We should look around studies of deformable component assembly. Robotic manipulations of deformable objects, such as cables, fabric, or foam rubber, have been extensively discussed in [18]. One of the difficult problems is recognizing the structure of deformable components. Matsuno applied topological model and knot theory to recognize a wire structure by a single camera [19]. Yasuno utilized 3-D range sensor and force sensor for recognizing connector with flexible cable [20]. Jian utilized image markers attached on wire harness for recognizing wire structures and connector orientations in practical scenario such as a car production line [21]. Another difficult problem is how to realize a secured mating between deformable objects. Huang constructed a force–displacement model of successful mating process through experiment with typical connectors and developed a fuzzy-based classifier for fault detection and diagnosis [22]. Fei proposed error recovery strategies for connectors mating based on force sensor [23]. These approaches give less weight to precision because positional error can be cancelled by deformable components. So, they are not suitable for our targeting precise assembly.

The purpose of this research is to develop a new insertion method that enables a versatile robot system to execute assembly task with the clearance smaller than $10\,\mu$m. The concrete target task presented in this paper is that a robotic hand holds a deformable thin ring and put it around a shaft (see Fig. 1). This task appears frequently in manufacturing scenes including fabrication of cylindrical components, such as a piston and a piston ring in reciprocating engine, a rotor and a shaft bushes

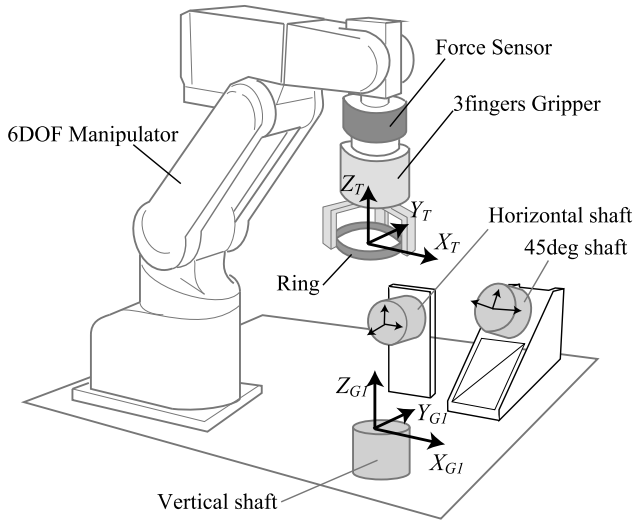

Fig. 1. Insertion process by 6-DOF manipulator.

of flat motor or hard dDisk drive (HDD), a lens and a flange of zoom lens system, and so on. The inside dimension of the ring and the outside dimension of the shaft are $\phi 50\mathrm{H8}(50^{+0.039}_{0.000})$ and $\phi 50\mathrm{g7}(50^{-0.009}_{-0.034})$, respectively. Therefore, the narrowest clearance is $9\,\mu$m in our target assembly task. In order to accomplish the assembly target, we propose a passive alignment principle (PAP) for reduction of positioning errors of robot and a new mating and insertion algorithm using the PAP.

The most significant difference between the conventional method and our proposed method is where the compliance is realized. Most of all conventional studies assumed that a robot hand holds a peg tightly, or else the peg wobbles due to its long unbalanced shape. Therefore, the compliance, which is absolutely necessary for assembly without jamming, is realized on a list (RCC device) or joints of robot arm (compliance control). In the assembly of electric connectors case, the deformable plastic connectors realize the compliance. On the other hand, our proposed method accepts a loose grip because the ring is usually short in axial direction and easy to be dealt with. The loose grip approach makes it possible to set compliance on contact point, and the one of examples is the PAP.

In Section II, the mechanism and the limitation analysis of PAP are described. In Section III, a novel mating algorithm using PAP is given, and in Section IV, the proposed PAP-based insertion algorithm is evaluated in repeatable mating and insertion experiments. Then, the validity is discussed on the basis of the experimental results. In Section V, the generality of the PAP is discussed from theoretical and experimental aspects. In Section VI, we summarize this paper and mention our future work.

II. Passive Alignment Principle

A. Mechanism

The mechanism of the PAP is simple in spite of its lots of advantages. Fig. 2 shows that rings and shafts are aligned in line by the effect of the PAP.

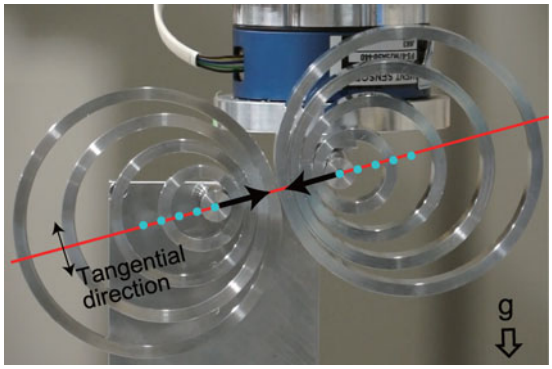

Fig. 2. PAP is working so that the rings lie on a straight line of perpendicular direction. The PAP also works for aligning circular peg and hole. For more information, see the supplementary video file.

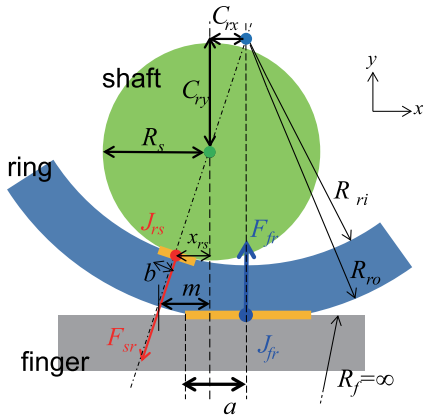

Fig. 3. Mechanism of PAP.

Two parallel shafts hang four rings respectively. The one shaft is fixed on a table and another shaft is fixed on a robot arm. The robot arm forces two shafts to come closer. When the distance between the two shafts is not close enough, the centers of rings have some displacements in tangential direction because of gravitational force. When the shafts come close enough, the displacement of each ring comes to zero, and then the center point of the rings, the center of shafts, and their contact points lie in a straight line.

B. Limitation Analysis based on Hertz Stress

Assuming that materials of the finger, ring, and shaft are rigid bodies, the displacement of tangential direction decreases to zero. However, considering the precise mating process, the effect of elastic deformation cannot be neglected. The remaining pose error after the PAP effect is analyzed here.

When each part is elastic, a contacting surface is formed due to the deformation of part (see Fig. 3). The size of the deformation area is given from Hertz's contact stress formulation [24], [25]. Considering a contacting surface between the finger and the ring, the width $2a$ is given as follows:

$$a = \sqrt{\frac{2F_{fr}}{\pi l}\left(\frac{1-\nu_r^2}{E_r}+\frac{1-\nu_f^2}{E_f}\right)\Big/\left(\frac{1}{R_{ro}}+\frac{1}{R_f}\right)}, \quad (1)$$

where E denotes Young's modulus of each material, ν denotes the Poisson ratio of them, l denotes the contact length (vertical to paper), $1/R$ denotes the curvature, and F_{rp} denotes the force from the finger to the ring. When the contact surface is plane as shown, $1/R$ is zero by the definition of Hertz's formulation.

In Fig. 3, the ring receives contact forces F_{fr} from the finger and F_{sr} from the shaft. When the center of the ring has a gap C_{rx} from the shaft center in x-direction, F_{fr} and F_{sr}, which has an angle, impinge on the ring as rotational moment to reduce C_{rx}. However, in the case that the extended line of the F_{sr} crosses the area of contact surface, the rotational moment presumably decreases. Therefore, the remaining pose error is given as follows:

$$C_{rx} + m \le a. \quad (2)$$

Let the origin locate on the center of the shaft, then the center of the ring is (C_{rx}, C_{ry}). The lateral face of the shaft and the inner face of the ring are expressed as follows:

$$\begin{cases} x^2 + y^2 = R_s^2 & (3a) \\ (x - C_{rx})^2 + (y - C_{ry})^2 = R_{ri}^2. & (3b) \end{cases}$$

From the relation of ratio of length, following equation is derived:

$$R_s : \left(R_{ro} - \sqrt{C_{rx}^2 + C_{ry}^2}\right) = |x_{rs}| : m. \quad (4)$$

From the contact point $J_{rs}(x_{rs}, y_{rs})$, which comes from (3a) and (3b), and from (4), m can be derived as follows:

$$m = C_{rx}\left(R_s + R_{ro} - R_{ri}\right). \quad (5)$$

By substituting a and m into (2), the remaining pose error after the PAP effect can be derived as follows:

$$C_{rx} \le \frac{R_{ri} - R_s}{R_{ro}}\sqrt{\frac{2R_{ro}F_{fr}}{\pi l}\left(\frac{1-\nu_r^2}{E_r}+\frac{1-\nu_f^2}{E_f}\right)}. \quad (6)$$

For example, in the case, where the diameter of shaft is $\phi 50$, the ring material is acrylonitrile-butadiene-styrene (ABS) ($E_r = 2.0 \times 10^9\ \mathrm{N/m^2}$, $\nu_r = 0.35$), the material of finger is aluminum (Al) ($E_f = 70 \times 10^9\ \mathrm{N/m^2}$, $\nu_f = 0.34$), the contact length is $l = 0.5\,\mathrm{mm}$, the maximum of remaining pose error is $C_{rx}^* = 0.0072\,\mu\mathrm{m}$. This is negligibly small to the narrowest clearance $9\,\mu\mathrm{m}$. So, the remaining pose error of the PAP effect has no influence on mating.

III. Insertion Algorithm Based on PAP

A. Algorithm Overview

It is an important matter how to treat the issues of accuracy and deformation. In this algorithm, the issue of accuracy is solved by the PAP and the issue of deformation is solved by the process of relaxing the grip force without dropping the ring. Including these key techniques, our proposed algorithm consists of four processes. The flowchart of whole process of insertion algorithm is shown in Fig. 4. The graphical explanation of insertion algorithm is shown in Fig. 5. First, details of the algorithm are described with each step, then the requirements of initial state

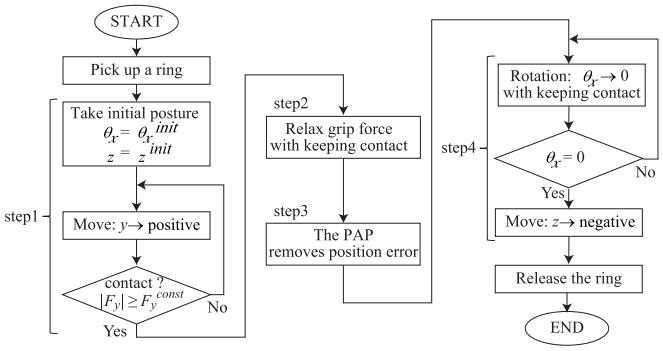

Fig. 4. Flowchart of the PAP-based insertion algorithm.

and the compliance control for this algorithm are described in Sections III-C and III-D, respectively.

B. Details of the Algorithm

1) Step 1 (Approach): The robot hand holds a ring firmly and takes its initial posture, where the angle between the central axis of the ring and the shaft is θ_x^{init}, and the lowest point of the ring is located in the lower portion by z^{init} with respect to the top surface of the shaft. When the robot hand moves to the shaft, the ring contacts the shaft first in its inner edge (J_{rs}) but outer edge by virtue of initial posture. When the force sensor value meets the condition $|F_y| \geq F_y^{\text{const}}$, the system detects contact and starts compriance control. At this stage, there is a positioning error δx in the x-axis direction. The acceptable range of θ_x^{init} and z^{init} are calculated in Section III-C.

2) Step 2 (Relaxing Grip Force): After the ring contacts the shaft in its inner edge (J_{rs}), Step 2 starts. The robot hand relaxes the grip force and the three fingers of robot hand moves outward. At the same instance, the robot manipulator makes small movement toward the shaft by the distance which is same to the finger 1 movement. This movement keeps contact of the ring with the shaft. Hence, the ring is pinched by the finger and the shaft so as not to fall down even if the grip force disappears.

3) Step 3 (PAP): Deactivating off the grip force enables the ring to move freely in the horizontal direction. Therefore, the PAP performs well and the position error δx comes to zero so that the center point of ring (C_r) and the center point of shaft (C_s) get together. Additionally, the disappearing of grip force restores circular shape of the ring from deformation. The issue of robot accuracy as well as the issue of ring deformation are solved here.

4) Step 4 (Mating and Insertion): Since the robot manipulator rotates the robot hand, the θ_x comes to zero with keeping the contact of ring and shaft at J_{rs}. Though the ring is not restrained by fingers in horizontal direction, the top face of ring is pressed by fingers so as to rotate with the robot hand. Fig. 5 shows the finger's action clearly. This movement is realized by the compliance control with force feedback described in Section III-D. After rotation movements, the robot manipulator goes straight in shaft direction to insert the ring deeper. The fingers do not hold the ring but just press it on the top surface, neither jamming nor wedging occurs.

C. Requirements: The Allowance Position Range of Initial State

Here, we derive the allowance ranges of θ_x^{init} and z^{init}. Let D_r and D_s denote the internal diameter of ring and the diameter of shaft, respectively. Both of the edges are chamfered with $C(d_{\text{ch}})$ (see Fig. 6).

First, the step 1 is considered. In order to prevent the ring and the shaft from contacting on their chamfer

$$2d_{\text{ch}} < z^{\text{init}} \tag{7}$$

must be met. The relation between θ_x^{init} and z^{init} is given from the condition that the internal side face of ring contacts with the lateral side of shaft as follows:

$$z^{\text{init}} < \frac{1}{2} D_r \sin(\theta_x^{\text{init}}). \tag{8}$$

The lower limit of θ_x^{init} is determined from (7) and (8)

$$\sin^{-1}\left(\frac{4d_{\text{ch}}}{D_r}\right) < \theta_x^{\text{init}}. \tag{9}$$

There is no geometrical upper limit θ_x^{init}, it should be as small as possible considering the PAP mechanism.

Next, we consider step 4. The condition that the horizontal projection of the internal diameter of ring is larger than the diameter of shaft is given with the ring angle at the moment of mating: $\theta_x^{\text{mate}} < (\theta_x^{\text{init}})$

$$D_s < D_r \cos\left(\theta_x^{\text{mate}}\right) = D_r \cos\left(\sin^{-1}\left(\frac{z^{\text{init}}}{D_r}\right)\right). \tag{10}$$

From this, the upper limitation of z^{init} is derived as follows:

$$z^{\text{init}} < D_r \sin\left(\cos^{-1}\left(\frac{D_s}{D_r}\right)\right). \tag{11}$$

Comparing (8) and (11), the condition defined by (8) is more stringent. Hence, the limitation of z^{init} is determined as follows:

$$2d_{\text{ch}} < z^{\text{init}} < \frac{1}{2} D_r \sin(\theta_x^{\text{init}}). \tag{12}$$

Next, we consider the allowance range of δx. The δx is equal to the C_{rx} in Fig. 3. Let us suppose that the ring is tilted slightly; the tilt angle is θ_x. Then, the internal curved edge of the ring is given as parametric equations with a parameter u ($0 \leq u < 2\pi$) and expressed as follows:

$$\begin{cases} x = C_{rx} + R_{ri}\cos(u) & \text{(13a)} \\ y = C_{ry} + R_{ri}\sin(u)\cos(\theta_x) & \text{(13b)} \\ z = C_{rz} - R_{ri}\sin(u)\sin(\theta_x). & \text{(13c)} \end{cases}$$

The ring edge is required to contact the shaft on side, neither on edge nor on top face, so that the ring is subjected to the PAP effect. Based on appropriate contact conditions of the ring and shaft, the allowance range of δx together with the ranges of θ_x and z^{init} can be calculated using (9) so that the allowance diagram is obtained. A specific example of the allowance diagram, in the case that ϕ_S is 50.013C0 and ϕ_R is 50.019C0, is shown in Fig. 7. The hatching region represents the allowance region of δx and z^{init}. The positioning error span of the robot manipulator, which is aiming $x = 0.0$ and $z^{\text{init}} = 0.5$, is drawn as white

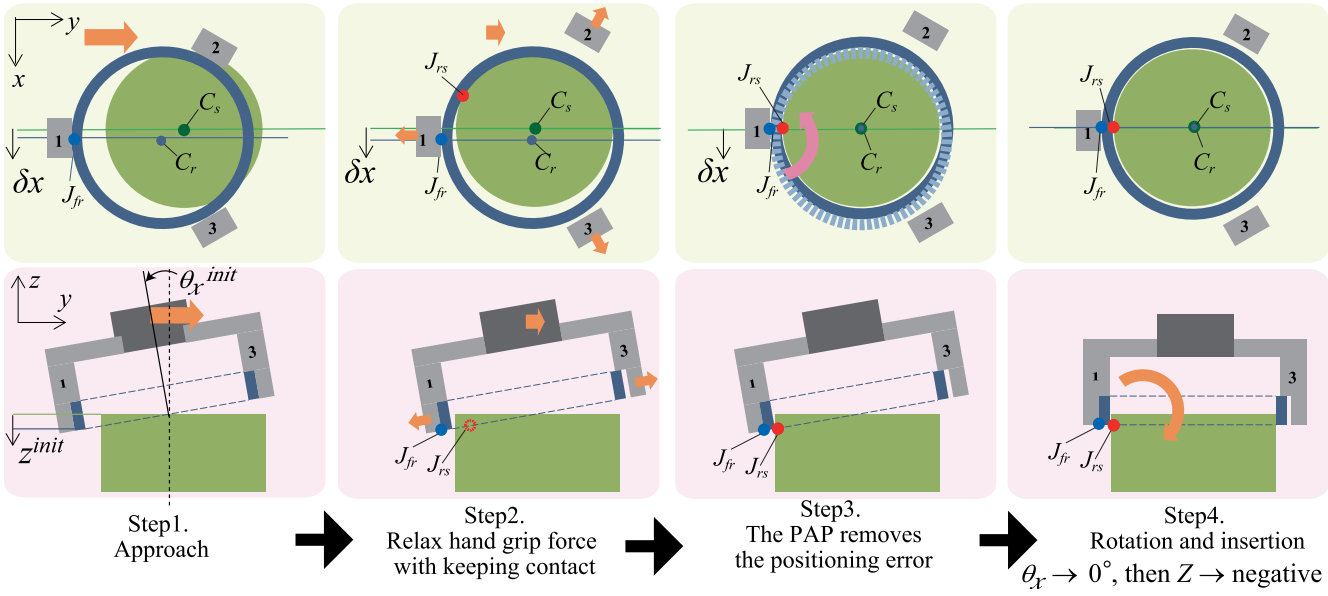

Fig. 5. Graphical explanation of the insertion algorithm.

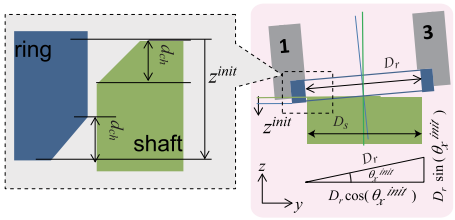

Fig. 6. Closeup of the contact point of the ring and the shaft.

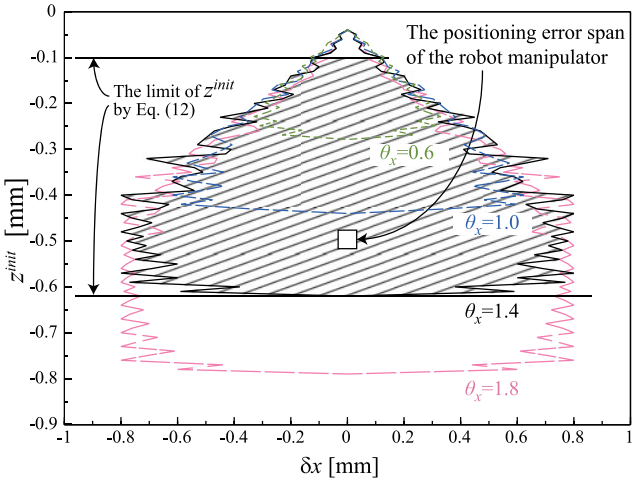

Fig. 7. Calculated allowance diagram of the case that ϕ_S is 50.013C0, and ϕ_R is 50.019C0.

square. So, the allowance region clearly covers the positioning error span of the robotic manipulator.

D. Compliance Control With Force Feedback

The compliance control, the block diagram of which is shown in Fig. 8, is applied for robotic manipulator. The $K_s = \mathrm{diag}(0, 100, 100, 0, 0, 0)\,\mathrm{N/m}$ is a stiffness matrix and the $K_f = (0, 0.15, 0.1, 0, 0, 0)\,\mathrm{m/N \cdot s}$ is a gain matrix for force control. The compliance center is placed near the fingertips. This enables the manipulator to have compliance in the directions of y-axis and z-axis, and to perform the mating action with keeping contact force between ring and shaft.

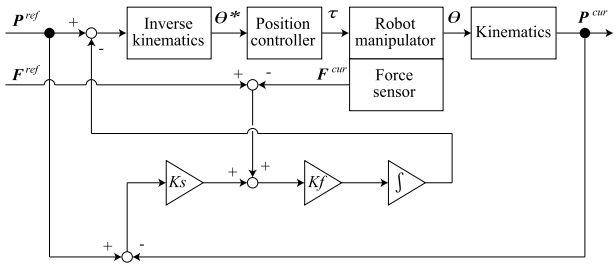

Fig. 8. Block diagram of robot control with force feedback.

IV. Experimental Study

A. Environment and Conditions

The experimental environment is shown in Fig. 9. The robot system consists of a 6-DOF manipulator (RV1A, Mitsubishi Electric Corporation), a control box (CR1, Mitsubishi Electric Corporation), a 1-DOF three-fingers gripper (ESG1-ST, TAIYO Ltd.), and a six-axis force sensor (IFS-67, NITTA Corporation) placed between the manipulator and the gripper. The control box measures and controls joint angles of manipulator. The conversion calculations between joint space and Cartesian space are executed in the control box. The control box, the gripper, and the force sensor are connected to Windows XP machine (Core i7, 3 GB memory) via TCP/IP communication, USB port, and special Ethernet-based communication, respectively. The sample time of the system is around 7 ms.

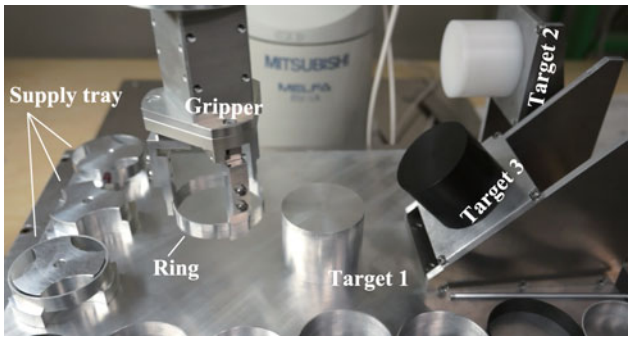

Fig. 9. Experimental environment.

There are three target shafts in the work space. The target 1 is an Al shaft fixed on the flat table. The target 2 is a polyoxymethylene (POM) shaft fixed on the vertical base. The target 3 is a polycarbonate glass fiber (PCGF) shaft fixed on the inclined base so that the axial direction of the shaft inclines at a 45° angle. There are three ring-supplying trays. They enable the robotic manipulator system to pick up a ring properly before each assembly process.

We prepared four materials: Al, PCGF, ABS, and POM so as to validate the applicability of various materials. More than five rings per material were machined, and the smallest one of each material was used for experiments. Also, one shaft per material were machined, and used for experiments. Details of the rings and shafts for the experiments are shown in Table II. For measuring the parts, we used a manual floating-type coordinate measuring machines (Crysta-Plus M544, Mitutoyo Corporation).

Through all experiments, the initial postures of ring were all the same, such that $\theta_x^{\text{init}} = 1.4°$ and $z^{\text{init}} = 0.5\,\text{mm}$. Also, the parameters for gripper control were fixed to the same values suited for Al-ring case, that the gripping force of the ring was $F_g = 7.0\,\text{N}$ and the width of finger movement at the step 2 was $h_d = 0.1\,\text{mm}$. The contact condition was set as $F_y^{\text{const}} = 1.5\,[\text{N}]$.

The calibration process for orienting the robot-coordinate system to the shaft-coordinate system was conducted before experiments. When the robot hand grabs the shaft while the robot arm is under compliance controll, the reaction forces F_x and F_y are measured. The arm position which gives smallest F_x and F_y is the center of shaft. By duplicating this operation at different height (z), the inclination between the two coordinate systems can be corrected. For z-axis orientation, a ring is used. The robot hand grabs a ring and touches the upper surface of shaft with the ring. The z-position where reaction force F_z generates is the height of shaft.

B. Procedures

1) Experiment I: In order to check the tolerance against pose errors, we examined the cases that the x-direction error δ_x were set to $0, 100, 200, \ldots$, and $800\,\mu\text{m}$ purposely. The sizes of ring and shaft in this experiment were equal to those of Section III-C, where the allowance diagram was calculated.

2) Experiment II: In order to validate the reliability for repeated tasks, we conducted 280 trials in total. They include not only the trials for target 1 but also the trials for target 2 and 3.

C. Results and Discussion

1) Experiment I: The snapshots in experiment I are shown in Fig. 10. The left one is the moment of step 2 and 3 when the PAP is working. The graphs of pose and force measured in respective cases in experiment I are shown in Figs. 11–14.

In the case of $\delta x = 0\,\mu\text{m}$, we can see the first contact between ring and shaft from the increasing of contact force, which expressed as decreasing of F_y, around $t = 500\,\text{ms}$. Then, the step 2 (relaxing grip force) begins and the contact force decreases due to the finger movement. However, the manipulator is moved immediately and the contact force is kept within the desired range by the compliance control. Although the effect of PAP is not shown in the graph, step 3 is considered to perform immediately after step 2. The rotation movement and the insertion movement in step 4 are shown as the decreasing of θ_x and decreasing of z, respectively. It takes about 3 s. to complete the one insertion task. The result graphs in the case of $\delta x = 100, \ldots, 500\,\mu\text{m}$ are similar to that of the case of $\delta x = 0$.

We are interested in the results that the x-direction error is on the border or out of the allowance range. Fig. 13 shows one of the typical results of border cases. Focusing on the reaction force F_z, we can see a drastic increase of F_z after rotation motion ($t = 1500\,\text{ms}$) and in the middle of insertion motion ($t = 2400\,\text{ms}$). This is because the PAP ends in failure and the position error remains. So, mild jamming occurs and causes the increase of reaction force in insertion direction. The insertion task itself has been successful, but the parts might be damaged by an extra reaction force.

Fig. 14 shows that the x-direction error is out of the allowance range. At first glance, it appears that up to step 4 (rotation) has been successful, but this is a wrong interpretation. In fact, the ring falls and gets stuck among the fingers and the shaft at step 2. The failures of step 2 and 3 are reflected in the trajectory of y, which seems different from the successful cases. Although the graphs presented here were only a part of our experiments, other trials resulted similar. We can say that the algorithm requirements derived in Section III-C are almost correct.

2) Experiment II: We got a 97.8% success rate in 280 trials including not only vertical insertion direction but also the horizontal and 45° of insertion directions. The detailed results are shown in Table II .

Let us consider the cause of failures in the case of POM-ring and ABS-ring to Al-shaft. The POM and ABS are softer than Al and easily deformed. However, the setting of gripping force and the width of finger movement are configured for Al-ring. So, the deformation of POM/ABS-rings still remains after step 2 and causes the failure.

On the other hand, the failure in the case of Al-ring to PCGF-shaft is caused by another reason. The PCGF-shaft is softer than Al-ring. Besides, the edge of Al-ring is not chamfered, and cuspidate. So, the edge of Al-ring cuts into the surface of PCGF-shaft in rare cases and leads to a failed insertion. Therefore, these failures can be avoided by setting the grip force proper for materials or arranging the angle θ_x and the contact force between the ring and shaft.

TABLE II
EXPERIMENTAL RESULTS OF LONG-TERM RELIABILITY

Inserting direction	Shaft Material	Shaft ϕ_S [mm]	Ring Material	Ring ϕ_R [mm]	Ring E [$\times 10^9$ N/m^2]	$C_R = (R_r - R_s)/R_r$	No. of trial	No. of success	Success Ratio [%]
			Al	50.019	70.0	0.00012	50	50	100
Vertical insertion	Al	50.013	PCGF	50.040	2.35	0.00054	50	50	100
			POM	50.141	2.00	0.00255	50	49	98
			ABS	50.210	1.12	0.00392	50	46	92
Horizontal insertion	POM	49.997	Al	50.019	70.0	0.00044	20	20	100
			POM	50.141	2.00	0.00287	20	20	100
45° insertion	PCGF	49.966	Al	50.019	70.0	0.00106	20	19	95
			PCGF	50.040	2.35	0.00148	20	20	100
Total	-	-	-	-	-	-	280	274	97.8

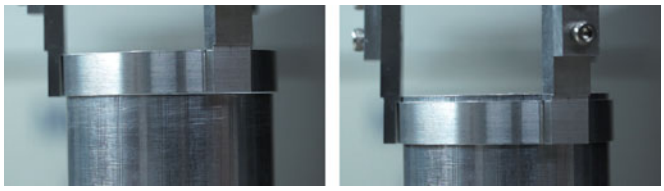

Fig. 10. Snapshots in experiment I: The left is the moment of PAP. The right shows the end of insertion.

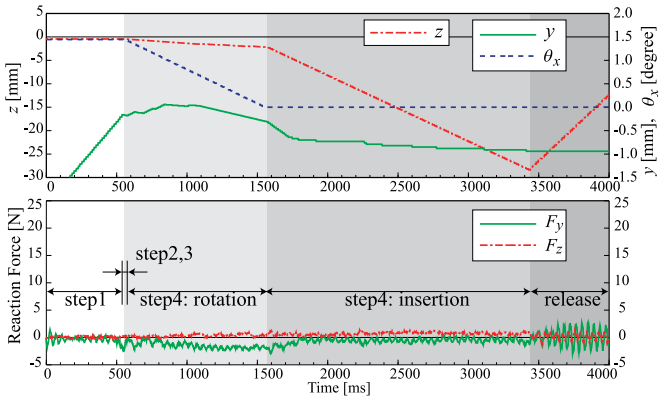

Fig. 11. Case $\delta x = 0\,\mu$m.

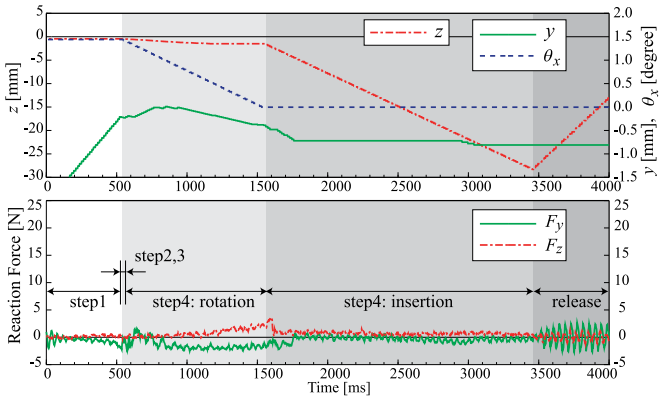

Fig. 12. Case $\delta x = 350.0\,\mu$m.

V. GENERALITY OF THE PAP

Because the PAP-based insertion method is new, it is helpful to discuss the generality of the method for future research. The

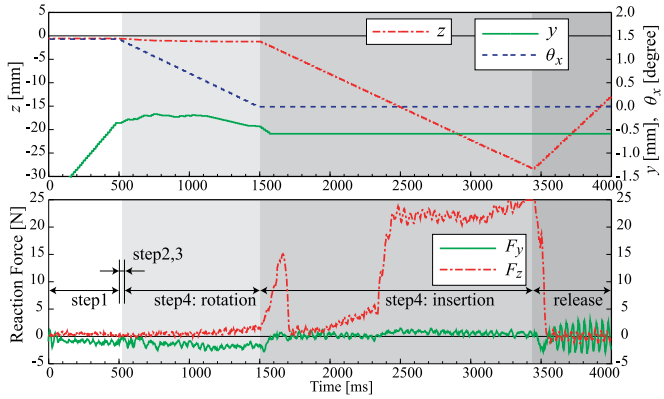

Fig. 13. Case $\delta x = 600\,\mu$m (near the border of allowance range).

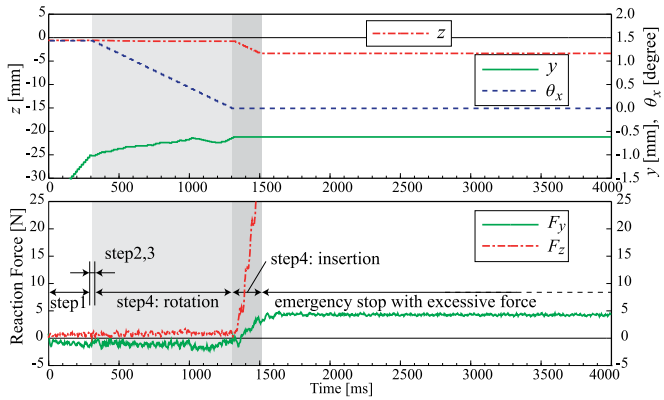

Fig. 14. Case $\delta x = 800\,\mu$m (out of the allowance range).

limitations and requirements of PAP-based insertion algorithm are as follows.

1) *Size:* The size/clearance limitation of ring and shaft is given as an allowance diagram like Fig. 7. We can select feasible sets of ring and shaft from the condition, which the allowance area cover the positioning error span of the robot manipulator.
2) *Shape:* The shapes of hole and peg must have rotational symmetries through any degrees because the PAP corrects the positioning error by rotating the ring. Briefly the shapes must be circular.
3) *Stiffness:* The ring must be stiff enough to be self-restoring when the grip force is decreased. The shaft

should also be hard to prevent the edge of ring from cutting into the surface.

4) *Weight:* The ring must be light enough not to be unstable while it is pinched by finger and shaft in Step 2 and Step 3.
5) *Contact force:* Though the PAP itself works with weak force, a certain force is required to keep the ring stable in step 2 and 3. The lower limit and upper limit are subject to the influence of the weight of ring and the stiffness of the shaft, respectively.
6) *Direction:* The PAP-based insertion algorithm can be applied for insertion tasks in all directions. Although the upside down insertion with PAP was not tested, it is thought to be possible. The points are Step 2 and Step 3, where the ring posture becomes unstable. Even if the ring posture is unstable, it is believed that the dimples of fingers (see Fig. 4) can hold a ring and prevent it from falling down as well as horizontal insertion.

VI. Conclusion

We proposed a PAP for robotic assembly with extremely narrow clearance. The PAP affects a contact point of two circular surfaces, such as a lateral face of shaft and an inner face of ring, and adjusts the ring position so that the center point of the ring orients to the center point of the shaft. We analyzed the mechanism of the PAP based on Hertz contact stress, and confirmed that the remaining errors after the PAP become smaller than $0.1\ \mu$m even if the ring or shaft are soft material like a plastic. We applied the PAP to an assembly problem, which a robotic hand holds a ring part and insert it in a shaft part, and also developed a mating and insertion algorithm based on the PAP. We calculated an allowance diagram of typical case as accuracy requirements of the algorithm, and confirmed that the accuracy requirements can be satisfied easily by a general 6-DOF robotic manipulator.

We validate our proposed PAP-based insertion algorithm with two experiments. The experiment we proved that the algorithm was tolerant to x-directional positioning error. The results supported the allowance diagram as algorithm requirements. The experiment II proved that the algorithm was reliable in repeated task. The algorithm failed only six times in 280 trials. The causes of failures have been elucidated, and they can be solved by adjusting parameters, such as the grip force, the width of finger movement, and the contact force.

Consequently, our proposed PAP-based insertion algorithm is tolerant to robot positioning error and reliable in repeated tasks, and enables a general 6-DOF robotic manipulator to complete a precise robotic assembly task with extremely narrow clearance, such as $6\ \mu$m.

The assembly between a ring and a shaft appears frequently during manufacturing scenes including fabrication of cylindrical components, such as a piston and a piston-ring in reciprocating engine, a rotor and a shaft bushes of flat motor or HDD, a lens and a flange of zoom lens system, etc. Although the PAP was invented in a problem setting that a robot hand hold a ring and put it around a shaft, it can also be applied for the case when a robot holds a shaft and inserts it in a hole. In that situation, investigations of allowable length and weight of shaft are next challenge. One of the future works, except for extending the limitations mentioned in Section V, is speeding up the whole process. This issue will be solved by tuning parameters suited for each task and utilizing a robot system with shorter control cycle.

References

[1] Y. Yamamoto, T. Hashimoto, T. Okubo, and T. Itoh, "Measurement of force sensory information in ultraprecision assembly tasks," *IEEE/ASME Trans. Mechatronics*, vol. 7, no. 2, pp. 186–189, Jun. 2002.

[2] L. Wang, S. Keshavarzmanesh, H. Y. Feng, and R. O. Buchal, "Assembly process planning and its future in collaborative manufacturing: A review," *Int. J. Adv. Manuf. Technol.*, vol. 41, no. 1, pp. 132–144, 2009.

[3] F. Duan, J. T. C. Tan, J. G. Tong, R. Kato, and T. Arai, "Application of the assembly skill transfer system in an actual cellular manufacturing system," *IEEE Trans. Autom. Sci. Eng.*, vol. 9, no. 1, pp. 31–41, Jan. 2012.

[4] D. E. Whitney, "Quasi-static assembly of compliantly supported rigid parts," *ASME J. Dyn. Syst. Meas. Control*, vol. 104, pp. 65–77, 1982.

[5] P. C. Watson, "Remote center compliance system," U.S. Patent 4 098 001, Jul. 4, 1978.

[6] S. H. Drake and S. N. Simunovic, "Compliant assembly system evice," U.S. Patent 4 155 169, May 22, 1979.

[7] S. Lee, "Development of a new variable remote center compliance (VRCC) with modified elastomer shear pad (ESP) for robot assembly," *IEEE Trans. Autom. Sci. Eng.*, vol. 2, no. 2, pp. 193–197, Apr. 2005.

[8] Y. Band, K. Lee, J. Kook, W. Lee, and I. Kim, "Micro parts assembly system with micro gripper and RCC unit," *IEEE Trans. Robot.*, vol. 21, no. 3, pp. 465–470, Jun. 2005.

[9] M. H. Raibert and J. J. Craig, "Hybrid position/force control of manipulators," *ASME J. Dyn. Syst. Meas. Control*, vol. 103, no. 2, pp. 126–133, 1981.

[10] Y. Li, "Hybrid control approach to the peg-in-hole problem," *IEEE Robot. Autom. Mag.*, vol. 4, no. 2, pp. 52–60, Jun. 1997.

[11] N. Hogan, "Impedance control. Part I—Theory, Part II—Implementation and Part III—Applications," *ASME J. Dyn. Syst. Meas. Control*, vol. 107, pp. 1–23, 1985.

[12] M. Koide, T. Kuno, and C. Hayashi, "Force control of a 6-articulated manipulator (in Japanese)," *R & D Rev. Toyota CRDL*, vol. 27, no. 4, pp. 25–35, 1992.

[13] S. Joo, M. Shimomura, D. Sekimori, Y. Masutani, and F. Miyazaki, "Precise mating algorithm using articulated robot manipulators (in Japanese)," *JSME Trans. Series C*, vol. 61, no. 584, pp. 308–314, 1995.

[14] T. Tsumugiwa, A. Sakamoto, R. Yokogawa, and K. Hara, "A control strategy for human-robot cooperative carrying and peg-in-hole task (in Japanese)," *JSME Trans. Series C*, vol. 70, no. 689, pp. 69–76, 2004.

[15] J. A. Marvel, W. S. Newman, D. P. Gravel, G. Zhang, J. Wang, and T. Fuhlbrigge, "Automated learning for parameter optimization of robotic assembly tasks utilizing genetic algorithms," in *Proc. IEEE Int. Conf. Robot. Biomimet.*, Bangkok, Thailand, Feb. 21–26, 2009, pp. 179–184.

[16] S. Ando, R. Nagai, and Y. Inoue, "Automatic damping tuning of impedance control for assembly task (in Japanese)," *J. Robot. Soc. Japan*, vol. 29, no. 7, pp. 564–572, 2011.

[17] A. Stolt, M. Linderoth, A. Robertsson, and R. Johansson, "Adaptation of force control parameters in robotic assembly," presented at the IFAC Int. Symp. Robotics Control, Dubrovnik, Croatia, Sep. 5, 2012.

[18] D. Henrich and H. Wörn, *Robot Manipulation of Deformable Objects*. Berlin, Germany: Springer-Verlag, 2000.

[19] T. Matsuno, D. Tamaki, F. Arai, and T. Fukuda, "Manipulation of deformable linear objects using knot invariants to classify the object condition based on image sensor information," *IEEE/ASME Trans. Mechatronics*, vol. 11, no. 4, pp. 401–408, Aug. 2006.

[20] K. Yasuno, R. Haraguchi, K. Shiratsuchi, Y. Domae, H. Okuda, A. Noda, K. Sumi, T. Fukuda, S. Kaneko, and T. Matsuno, "A robotic assembly system capable of handling flexible cables with connector," in *Proc. Int. Conf. Mechatronics Autom.*, 2011, pp. 893–897.

[21] X. Jiang, K. Koo, K. Kikuchi, A. Konno, and M. Uchiyama, "Robotized assembly of a wire harness in a car production line," *Adv. Robot.*, vol. 25, nos. 3/4, pp. 473–489, 2011.

[22] J. Huang, T. Fukuda, and T. Matsuno, "Model-based intelligent fault detection and diagnosis for mating electric connectors in robotic wiring harness assembly systems," *IEEE/ASME Trans. Mechatronics*, vol. 13, no. 1, pp. 86–94, Feb. 2008.
[23] C. Fei, F. Cannella, H. Sasaki, C. Canali, and T. Fukuda, "Error recovery strategies for electronic connectors mating in robotic fault-tolerant assembly system," in *Proc. IEEE/ASME Int. Conf. Mechatronics Embedded Syst. Appl.*, 2014, pp. 1–6.
[24] H. Hertz, "Uber den kontakt elastischer korper (in German)," *J. Reine Angew. Mathematik*, vol. 92, pp. 156–171, 1881.
[25] S. P. Timoshenko and James M. Gere, "Hertz contact stress," in *Theory of Elasticity* (Classic Textbook Reissue Series), New York, NY, USA: McGraw-Hill, 1970.

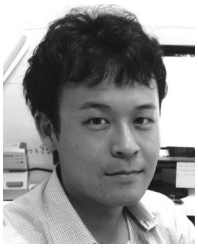

Junji Takahashi (M'08) received the B.E., M.E., and Ph.D. degrees in engineering from Nagoya University, Nagoya, Japan, in 2005, 2007, and 2010, respectively.

He was a Research Fellow of GCOE (Cybernics) at the Graduate School of Systems and Information Engineering, University of Tsukuba from April 2010 to March 2012, and a Postdoctoral Research Fellow at Nagoya University from April 2012 to March 2013. He is currently an Assistant Professor at Aoyama Gakuin University, Tokyo, Japan. His research interests include mechatronics, distributed autonomous robotic systems, robotics for disaster response, factory automation, human–robot interaction, and biosignal processing.

Dr. Takahashi is a Member of the RSJ and the Society of Instrument and Control Engineers (SICE). He received the Best Paper Award at the 9th International Symposium on Distributed Autonomous Robotic Systems, and a prize of encouragement from the Chubu Branch of the SICE in 2012.

Tomoya Fukukawa received the B.E. and M.E. degrees in engineering from Nagoya University, Nagoya, Japan, in 2011 and 2013, respectively, where he is currently working toward the Ph.D. degree with the Department of Mechanical Science and Engineering.

His research interests include factory automation and agricultural robotics.

Toshio Fukuda (M'83–SM'93–F'95) received the Graduation degree from Waseda University, Tokyo, Japan, in 1971, and the M. Eng. and Dr. Eng. degrees both from the University of Tokyo, Tokyo, in 1973 and 1977, respectively, after studying at Yale during 1973–1975.

He joined the National Mechanical Engineering Laboratory in Japan and also at the University of Stuttgart as a Research Scientist. He joined the Science University of Tokyo in 1981, and then joined the Department of Mechanical Engineering, Nagoya University, Japan, in 1989. Currently, he is a Professor of the Beijing Institute of Technology and Nagoya/Meijo University.

He was the President of the IEEE Robotics and Automation Society during 1998 1999, the IEEE Director Division X Systems and Control during 2001–2002, the Founding President of the IEEE Nanotechnology Council during 2002–2005, the Editor-In-Chief (EiC) of the IEEE/ASME TRANSACTIONS ON MECHATRONICS during 2000–2012, and the IEEE Region 10 Director during 2013–2014. He has been the EiC of the Robomech Journal of Springer since 2013, a Member of the Science Council of Japan during 2008–2014, and a Member of the Academy of Engineering of Japan since 2013.